P. Lorenzino et alii, Frattura ed Integrità Strutturale, 41 (2017) 191-196; DOI: 10.3221/IGF-ESIS.41.26

Focused on Crack Tip Fields

Influence of forging conditions on the fatigue mechanisms of low alloy steels: a 3D study

Pablo Lorenzino, Jean-Yves Buffiere, Catherine Verdu

INSA Lyon MATEIS Bat Saint Exupery 25 Av. Jean Capelle F-69621 Villeurbanne Cedex France

jean-yves.buffiere@insa-lyon.fr

ABSTRACT. The influence of forging conditions on the propagation of physically small fatigue cracks has been studied for two high strength steels. Two surface conditions were produced after the forging process. The subsurface microstructure of the materials has been characterized by EBSD. Small samples extracted from the original specimens were used to perform in situ fatigue tests monitored by high resolution synchrotron X-ray tomography. Fatigue cracks were initiated from an artificial defect (100 µm wide x 50 µm deep) introduced in the forging skin by laser machining.

3D images of the initiation and growth of those physically small fatigue cracks have been obtained. It was found that the presence of a shot-blasted skin containing a hardness and microstructure gradient influences the 3D crack shape during propagation in comparison with the materials without material properties gradient. The 3D crack shapes are rationalized in terms of crack closure effects induced by the forging processes, close to the surface.

KEYWORDS. Short cracks; 3D propagation; Crack closure; Synchrotron X-ray tomography; Forging.

Citation: Lorenzino, P., Buffiere, J.-Y., Verdu, C., Influence of forging conditions on the fatigue mechanisms of low alloy steels: a 3D study, Frattura ed Integrità Strutturale, 41 (2017) 191-196.

Received: 28.02.2017
Accepted: 15.04.2017
Published: 01.07.2017

INTRODUCTION

With the enforcement, in the very near future, of new European regulations in terms of fuel consumption, car manufacturers have put a large effort in trying to reduce the weight of vehicles in the last ten years. This has led to a global increase of the load level experienced by many components in the body, the panels, the wheels or the engine of cars. Being able to accurately predict the fatigue life of those components has now become a key issue for keeping the same trend and reducing the vehicle weight further. A good example, in the field of metallic components, is given by the connecting rods or crankshafts which are submitted to higher service load for a very large number of cycles. Although it is well accepted that the methods used to produce such components (mainly hot and cold forging) have a strong effect on the material microstructure and, therefore, on their mechanical properties, the thermo-mechanical history experienced by the metals during processing is not accurately taken into account at the design stage leading to over conservative safety coefficients.

In this study, four different industrially relevant forging conditions have been studied for two different pearlitic or ferritic-pearlitic steels. The effect of the processing route on the materials microstructure and mechanical behavior has been first evaluated. The 3D propagation behavior of fatigue cracks growing from shallow artificial defect (*i.e.* growing mainly within the forged skin of the materials) has been obtained through in situ X-ray synchrotron tomography. The crack growth curves have been obtained for all materials and the effect of processing on crack growth behavior assessed.

EXPERIMENTAL

Materials

Four different forging condition of industrial relevance were investigated for two different steels. Cold forged cylindrical specimens produced with two different cross sectional area reduction (18 and 75 %) have been obtained for a 27MnCr5 ferritic-pearlitic steel [1]. A C70 pearlitic steel was also used to produce connecting rods through a four step hot forging process. Samples were extracted from the connecting rods directly in the as-forged condition or after a shot-blasted treatment applied in order to remove the scale [2].

Tab. 1 details the processes and the mechanical properties of the four different materials/conditions studied (hereafter simply called different *materials* with a greek numbering as shown in the table).

It can be seen from this table that the cold forging process produces a lower grain size than hot forging and that the grain size decreases with the level of reduction. When shot blasting is used (material IV) a grain size gradient is observed. EBSD observations reveal a 10 μm thick layer of extremely fine grains (< 1 μm); below this region a layer of heavily deformed grains is observed evolving gradually towards more equiaxed grains with an average size of 25 μm at a distance of 150-200 μm below the surface, where the unaffected bulk material begins. A gradient of mechanical properties is concomitantly observed with hardness values ranging from 350 HV at the surface to 280 HV at 400 μm below the surface. Finally, in the bulk material, a residual stresses gradient (measured by X-ray diffraction) with compressive stress values ranging from -500 MPa at the surface to 0 MPa at a distance of 400 μm below the surface was measured . More detailed information can be found in [2]

Synchrotron tomography experiments

In order to study the influence of the surface conditions induced by the finishing processes on the propagation of shallow fatigue cracks, small samples of 0.8 x 0.8 mm cross-sectional area were extracted at the surface of the forged components. The small cross section of the samples is the result of the large X-ray attenuation of Iron and the small voxel size required to detect accurately the small cracks [3]. Fig. 1 (a) and (b) show a schematic view of the fatigue samples extracted from the cold forged round bars (materials I and II) and from hot forged connecting rods (materials III and IV) by means of electro discharge machining.

Symbol	Material	Process	$\sigma_{0.2}$ (MPa)	Grain size (μm)
I	27MnCrFP	Cold Forged (18%)	730	15
II	27MnCrP	Cold Forged (75%)	1072	8
III	C70P	Hot Forged	800	25
IV	C70P	Hot Forged + shot blasting	800	1 to 25

Table 1: List of the materials and forging processes investigated with the corresponding mechanical properties and grain sizes. In material IV the shot blasting process produces a grain size gradient (see the text for details).

Residual stress measurements performed on the tomography samples showed values ranging from 0 to 20 MPa in samples of materials I, II and III. In the particular case of material IV, after spark machining the samples exhibited a curvature radius of 170 mm due to the presence of residual stress gradient. However, this curvature disappeared in the unloaded state after a few hundred fatigue cycles. Thus it can be concluded that the samples tested were free of residual stresses.

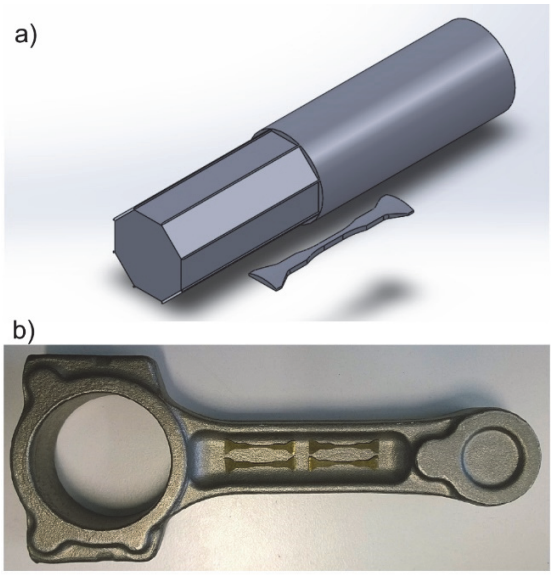

Figure 1: Miniature dog bone fatigue samples (cross section 0.8x0.8 mm^2) extracted at the surface of the forged materials from the cold forged bars (materials I and II) (a) or from the hot forged connecting rods (materials II and IV) (b).

Artificial defects that act as the initiation point of the fatigue cracks were introduced at the sample surface by laser machining as described elsewhere in the case of cast iron [4]. In this study the notch obtained has the shape of a narrow wedge of dimensions (depth/width/opening): 50x100-150x5 μm^3. It is shown schematically on Fig. 2.
In-situ fatigue tests were performed on ID19 beamline at the European Synchrotron Radiation Facility (ESRF). A "pink" X ray beam [5] with a photon energy of 60 keV is used with a Pco Edge CCD camera (2160 x 2560 pixels). The samples were cycled in situ using a dedicated fatigue machine mounted onto the rotation stage of the beamline [6]. Once crack initiation was detected (by inspection of the radiographs of the sample under load) tomographic scans (2000 projections, exposure time of 0.07s duration 3.68 min) were recorded regularly after a given number of cycles. The samples were scanned under maximum load in order to improve crack visibility. Uniaxial fatigue tests were carried out in pull-pull loading conditions with R=0.1. Reconstruction of the tomographic data was performed with a standard filtered back-projection algorithm. A 0.65 μm voxel size was obtained. Fiji and ParaView open softwares were used for post-processing the 3D images.

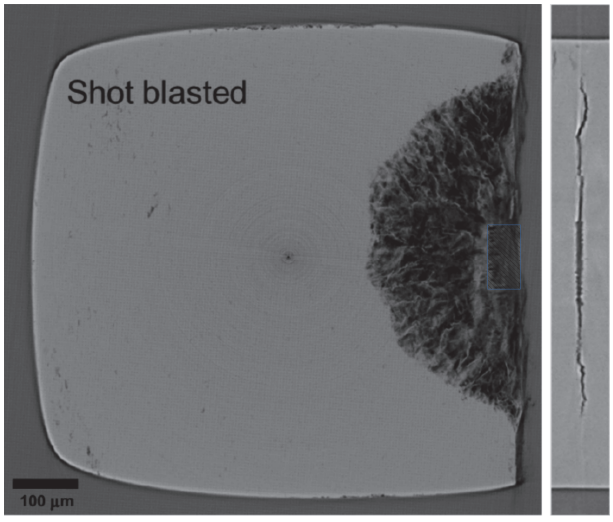

Figure 2: Left: Projected view (along the loading direction) of the crack shape for material IV (hot forged + shot blasted) after 66kcycles fatigue cycles at σ_{max} = 450 MPa R=0.1. The blue rectangle highlights the shape of the laser notch. Right: reconstructed slice showing the crack shape a few micrometers below the surface (loading direction horizontal).

RESULTS AND DISCUSSION

Tab. 2 summarizes the fatigue tests performed at the ESRF. Two tests were carried out in each material in order to have failures above and below 100.000 cycles. For material IV, five specimens were tested since in some cases the crack nucleated from a corner of the sample instead of the artificial defect.
The ability of tomography to detect accurately the size/shape of the cracks was assessed by comparing the surface crack size measured on the reconstructed images (*e.g.* right image on Fig. 2) with optical images obtained on the unbroken samples. In all cases a very good correspondence was observed (less than a few percent error). It was therefore possible to monitor accurately the 3D shape of the crack steadily propagating out of the artificial defect.

Material	Test	$\sigma_{max}/\sigma_{0.2}$	Cycles (x10^3)	Failure origin
I	1	0.62	61	notch
I	2	0.57	160	notch
II	3	0.52	71	notch
II	4	0.48	125	notch
III	5	0.52	30	sample corner
III	6	0.47	121	notch
IV	7	0.58	31	notch
IV	8	0.59	60	sample corner
IV	9	0.56	71.5	notch
IV	10	0.63	95	sample corner
IV	11	0.45	340	sample corner

Table 2: Summary of the fatigue tests carried out at the synchrotron.

Regarding the initiation stages, for the cold forged materials, a larger number of cycles was required to initiate a crack from the notch for the material with the largest strain level (material II). Regarding propagation, for all materials, both the crack surfaces and crack fronts were relatively flat/smooth showing no indication of strong interactions with the local microstructure (see for example Fig. 3 for an example of the crack fronts observed in material IV).

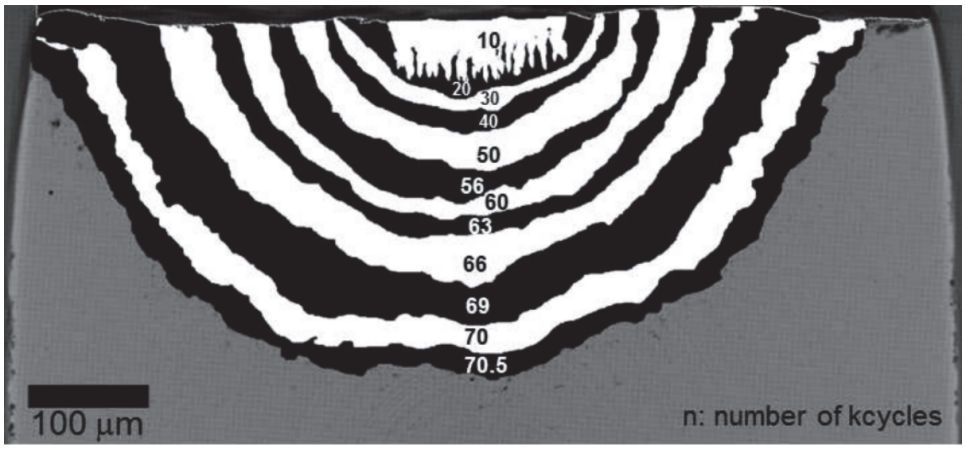

Figure 3: Crack front shapes for Material IV σ_{max} = 450 MPa, R=0.1. The shape of the crack fronts is relatively smooth indicating the absence of strong interaction with the local microstructure (*e.g.* grains).

Despite their small physical sizes, the cracks behave as "microstructurally long" fatigue cracks with continuously increasing growth rates. Fig. 4 shows a comparison of the crack growth rates as a function of ΔK for materials III and IV. In this figure the stress intensity factor values are based on the $(area)^{1/2}$ parameter proposed by Murakami [7].

It can be seen from this figure that the shot blasting effect has nearly no effect on the crack resistance of the two materials. The same results have been obtained when comparing materials I and II. A more sophisticated analysis taking into account the 3D shape of the cracks for the calculation of the Stress Intensity Factors (SIF) with the Raju & Newman analytical formulas [8] shows again no difference between the four materials in terms of crack growth rates.

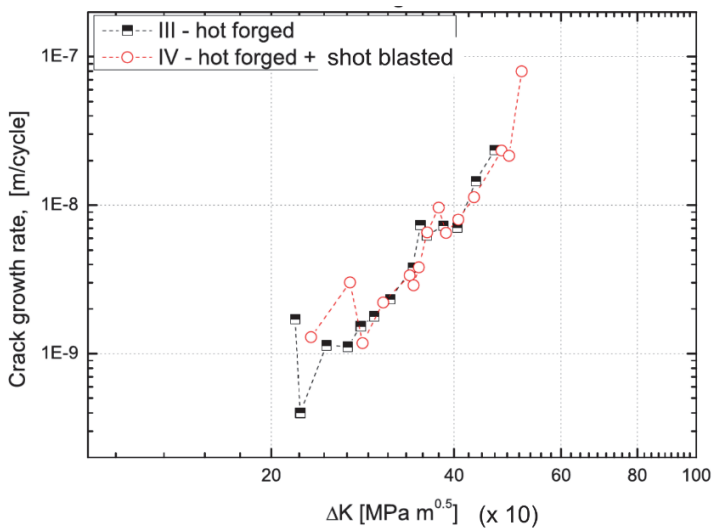

Figure 4: da/dN curves for materials III and IV. The SIF values are based on Murakami's $(area)^{1/2}$parameter.

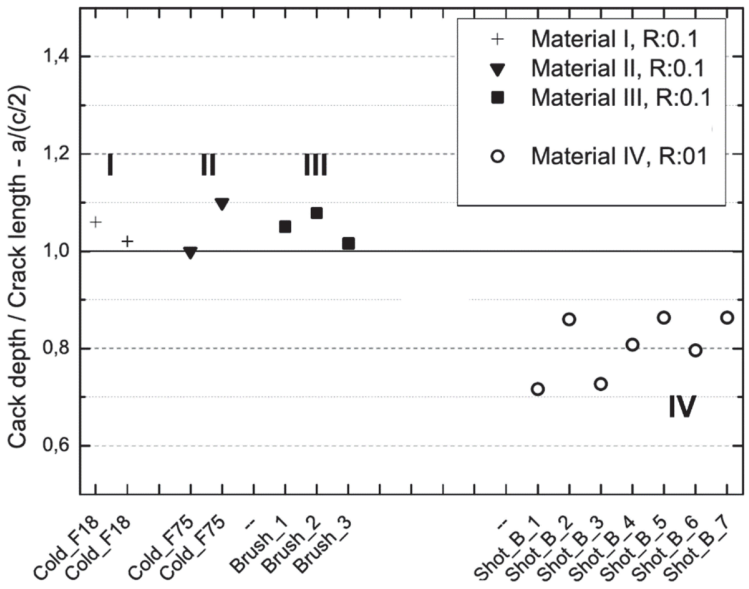

Figure 5: Crack aspect ratio for the four materials studied (several samples per materials).

One difference between the materials is observed when the crack *shape* is being considered. In case of material I, II and III the crack fronts acquire a semi-circular (penny) shape from a very early stage of propagation, conserving this geometry until final failure. In the case of material IV, however, the crack front acquires a semi-elliptical shape, a geometry which is maintained until final fracture. For materials I, II and III the crack intersects the surface with a 90 degree angle; this is not the case for material IV as observed on Fig. 3. Those differences are shown on Fig. 5 which gives a summary of the crack aspect ratio (depth/half surface length) for all materials: material IV is the only one which has a ratio below 1. A Raju & Newman analysis of the SIF values suggests that a penny shape correspond to a crack growing with an out of equilibrium shape that is to say a crack front along which K is not constant but higher at the surface. One explanation for this might be the "tunneling" effect of the crack which is well known for through cracks in CT samples (see for example [9]): a larger level of crack closure at the sample due to the larger plastic zone size "holds back" the crack front.

Although this has rarely been reported for 3D part-through cracks [10], this is consistent with the experimental observation of a grain size gradient at the surface of material IV. A smaller grain size restricts the plastic zone size (Hall Petch effect) and therefore the tunneling effect is reduced or even suppressed. Experiments at larger R ratio on materials III and IV (not shown here) tend to support this interpretation.

Conclusion

In situ fatigue tests monitored by synchrotron X-ray tomography have been carried out on four different forged materials (two different steels + two different forging processes). The residual stresses which have been measured in some of the bulk materials have been released in the fatigue samples because of their small size. For the experimental conditions investigated, it was found that there is no influence of the forging process on crack growth curves. Differences in crack front shapes have been observed for the material which has been shot blasted. Those differences are interpreted in terms of the modifications induced in the sub-surface microstructure by the forging processes: a reduction of sub-surface crack closure due to a local increase of the yield stress.

Acknowledgements

This project has been funded by the French Agence Nationale de la Recherche (Defisurf project). The authors want to thank Prof F.Morel and Dr. E.Pessard for fruitful discussions.

References

[1] Gerin, B., Pessard, E., Morel, F., Verdu, C.,Mary, A., Beneficial effect of prestrain due to cold extrusion on the multiaxial fatigue strength of a 27MnCr5 steel International Journal of Fatigue 92 (2016) 345–359. DOI: 10.1016/j.ijfatigue.2016.07.012

[2] Gerin, B., Pessard, E., Morel, F., Verdu, C., Influence of surface integrity on the fatigue behaviour of a hot-forged and shot-peened C70 steel component Materials Science & Engineering A 686 (2017) 121–133. DOI: 10.1016/j.msea.2017.01.041.

[3] Buffiere, J.-Y., Maire, E., Adrien, J., ·Masse, J.-P., Boller, E., In Situ Experiments with X ray Tomography: An Attractive Tool for Experimental Mechanics Experimental Mechanics 50 (2010) 289–305. DOI: 10.1007/s11340-010-9333-7.

[4] Lachambre, J.,Réthoré, J.,Weck, A., Buffiere, J.-Y., Extraction of stress intensity factors for 3D small fatigue cracks using digital volume correlation and X-ray tomography International Journal of Fatigue 71 (2015) 3–10. DOI: 10.1016/j.ijfatigue.2014.03.022.

[5] P. Willmott, P., An Introduction to Synchrotron Radiation: Techniques and Applications, John Wiley & Sons, (2011).

[6] Buffiere, J.-Y., Ferrie, E., Proudhon, H., Ludwig, W., Three dimensional visualisation of fatigue cracks in metals using high resolution synchrotron X-ray micro-tomography. Mater. Sc. Technol., 22(9)(2006) 1019–1024.

[7] Murakami Y., Metal fatigue: effect of small defects and non-metallic inclusions. Elsevier, (2002).

[8] Newman, J.C., Raju, I.S., An empirical stress-intensity factor equation for the surface crack Eng. Frac. Mech., 15 (1981) 185–192.

[9] Dawicke, D.S., Grandt, A.F., Newman, J.C., Three-dimensional crack closure behavior Engineering Fracture Mechanics, 36(1) (1990) 111-121.

[10] Ferrié, E., Buffiere, J.-Y., Ludwig, W., Gravouil, A., Edwards, L., Fatigue crack propagation: In situ visualization using X-ray microtomography and 3D simulation using the extended finite element method Acta Materialia, 54(4) (2006) 1111-1122. DOI: 10.1016/j.actamat.2005.10.053.